Journal of the Korean Society for Nondestructive Testing
Vol. 29, No. 4 (2009. 8)

Invited

Active-Sensing Lamb Wave Propagations for Damage Identification in Honeycomb Aluminum Panels

Eric B. Flynn*, R. Andrew Swartz*, Daniel E. Backman*, Gyuhae Park*† and Charles R. Farrar*

Abstract This paper presents a novel approach for Lamb wave based structural health monitoring(SHM) in honeycomb aluminum panels. In this study, a suite of three signal processing algorithms are employed to improve the damage detection capability. The signal processing algorithms used include wavelet attenuation, correlation coefficients of power density spectra, and triangulation of reflected waves. Piezoelectric transducers are utilized as both sensors and actuators for Lamb wave propagation. These SHM algorithms are built into a MatLab interface that integrates and automates the hardware and software operations and displays the results for each algorithm to the analyst for side by side comparison. The effectiveness of each of these signal processing algorithms for SHM in honeycomb aluminum panels under a variety of damage conditions is then demonstrated.

Keywords: Integrated Piezoelectric Transducer, Lamb Wave, Active Structural Health Monitoring, Honeycomb Structure

1. Introduction

The aerospace industry is increasingly utilizing honeycomb sandwich panels in a variety of applications. One application that is of particular interest to military planners is for unmanned aerial vehicles(UAVs), which are often constructed using a honeycomb panel skin (Fig. 1). The honeycomb panels used in UAVs are constructed from two thin aluminum or composite face sheets bonded to a honeycomb core; the face sheets carry nearly all of the bending loads whereas the core material supports the transverse shear loads. This configuration produces a panel that has a significantly higher strength to weight ratio than would a solid panel of the same material composition. However, given the distribution of loads in such panels, any damage to these panels can lead to a marked and substantial decrease in their load-carrying capability. Potential types of damage include cracking, buckling of the face sheets, buckling of the core, and delamination of the face material from the core. Potential sources of damage include overloading, foreign object impacts, corrosion, manufacturing defects, and fatigue (United States Department of Defense, 2000). According to the Government Accountability Office, the US Department of Defense spends $15.3 million for a single Global Hawk UAV (United States Government Office, 2000) and $3.3 million for a Predator UAV (United States Government Office, 2004). Given the high cost of replacement for a UAV, as well

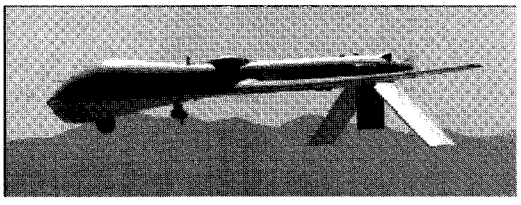

Fig. 1 Predator UAV - (photo courtesy of the Department of Homeland Security)

Received: May 25, 2009 *The Engineering Institute, Mail Stop T001, Los Alamos National Laboratory, Los Alamos, NM 87545, U.S.A, † Corresponding Author: gpark@lanl.gov

as the critical nature of the missions these vehicles perform, the availability of real-time information regarding the condition and serviceability of the aircraft is vital.

Structural health monitoring(SHM) is the process of measuring the dynamic response of a system and determining from these data the current state of the system's "health" in near real time. This process is typically carried out by comparing the dynamic response of an undamaged, baseline structure to that of the current, potentially damaged structure. The advantages of SHM include the possible detection of damage at its onset, before it has had a chance to propagate, thus reducing the potential for catastrophic failure (Farrar et al., 2001; Worden and Dulieu-Barton, 2004). In this paper, Lamb wave based SHM techniques are investigated for honeycomb aluminum panels. Since the 1960s, the ultrasonic research community has studied Lamb waves for the nondestructive evaluation of plate-like structures (Bourasseau et al., 2000). The advances in sensor and hardware technologies for efficient generation and detection of Lamb waves and the need to detect sub-surface damage in laminate composite structures has led to a significant increase in the use of Lamb waves for detecting defects in structures (Sohn et al., 2004; Lee and Staszewski, 2003; Ihn and Chang, 2004; Kessler et al., 2002; Diamanti et al., 2005a; 2005b; Diamanti et al., 2004; Diaz Valdes and Soutis, 2002)

Lamb waves are mechanical waves corresponding to vibration modes of plates with a thickness on the same order of magnitude as their wavelength. Lamb waves couple longitudinal and shear waves of plane strain within a plate that propagate in a variety of modes that are either symmetric or antisymmetric. To use Lamb waves for SHM, it is useful to have a waveform that is easily recognizable both before and after propagation through the plate. For Lamb waves, the wave speed is frequency dependent, making them dispersive where different frequency components travel at different velocities within the plate. To maximize the effectiveness of the SHM technique, it is useful to choose a driving frequency at which the various Lamb wave modes are temporally well spaced and at which the modes of interest are relatively non-dispersive (Kessler et al., 2002). Choosing a suitable driving frequency allows the receiving sensors to record the input signal with a minimal amount of interference. Furthermore, several methods have been proposed to enhance the interpretation of the measured Lamb wave signals to detect and locate structural damage. They are based on changes in wave attenuations using wavelets (Sohn et al., 2004; Kessler et al., 2002), time-frequency analysis (Ihn and Chang, 2004), wave reflections (Diamanti et al., 2005; Giurgiutiu et al., 2002), and time of flight information (Lemistre and Balageas, 2001).

In this study, a novel approach of integrating multiple data interrogation algorithms of Lamb wave propagations for SHM applications is presented. Contrary to most Lamb wave-based SHM techniques, which utilize only a single signal processing method for damage identification, a suite of three signal processing algorithms are employed and grouped into one package to improve the damage detection capability. This integration allows the analyst to configure the data acquisition system and display the results from each of three damage identification algorithms for side by side comparison. This side by side comparison of results simplifies the task of identifying the relative effectiveness and sensitivity of each algorithm. A brief description of the four algorithms used follows; The first method is based on a comparison of Lamb wave attenuation in a baseline undamaged (i.e., "healthy") plate to that of a potentially damaged plate test case; the second method uses a cross-correlation of the power spectral density of

the recorded response in the baseline condition to that of the test case; and the third method attempts to identify Lamb waves reflected from the point of damage and locate them using time-of-flight information and triangulation processes. By grouping a suite of algorithms into one package, this study contributes to and enhances the visibility and interpretation of the Lamb wave signals related to damage identification in a structure. Although this study focuses on the monitoring of honeycomb aluminum panels, the approach is intended that it can be adapted into a variety of structural health monitoring applications.

2. Experimental Setup and Procedures

The panels tested in this study are commercially available honeycomb aluminum panels that are composed of two aluminum face sheets bonded to an aluminum honeycomb core. The panels have dimensions in the equal length of 609.6 mm. Two panels are studied: one with a thickness of 6.35 mm and one with a thickness of 12.7 mm. The dimensional properties of the two panels are summarized in Table 1. The panels are suspended vertically by elastic cords during testing frame to approximate a free-free condition. The panels are instrumented with a regular array of 12.7 mm diameter-circular PZT transducers with 0.4 mm thickness. The 6.35 mm thick panel has a four by four (sixteen total) array of transducers spaced 180 mm apart in each direction, evenly spaced from the edges (Fig. 2(a, b, d)). The 12.7 mm thick panel has a three by three (nine total) array of transducers, also spaced 180 mm apart in each direction, allowing a greater edge distance for the outer PZT transducers (Fig. 2(c)). The PZT transducers are bonded on a single side of each panel using a quick-setting adhesive. The effects of the size

Table 1 Panel Dimensional Data

Plate Thickness (mm)	Cell Diameter (mm)	Density (kg/m3)	Face Sheet Thickness (mm)
6.35	9.53	529	0.508
12.7	12.7	36.8	0.813

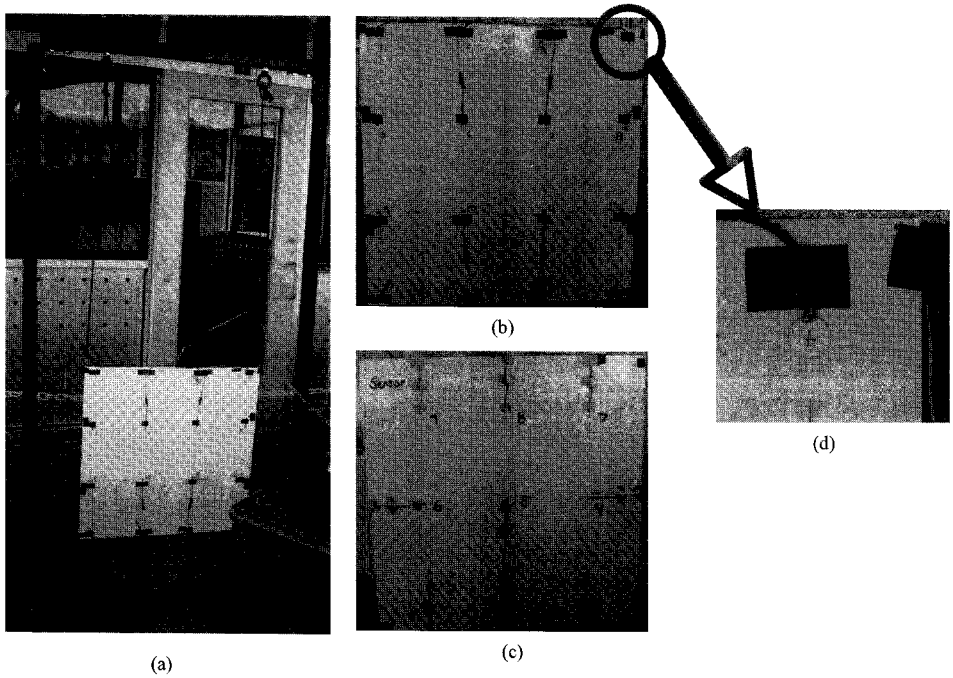

Fig. 2 Experimental setup used for testing: (a) panel support condition; (b) 6.35 mm panel; (c) 12.7 mm panel; (d) piezoelectric transducer

and the bonding layer on the Lamb wave propagation have been investigated by many researchers (Giurgiutiu, 2005; Park et al., 2006; Qing et al., 2006) In this study, the same size of the PZT patches were used to minimize the variability associated with the different dimension of PZT transducers and the integrity of the bonding conditions were assured using the newly developed sensor diagnostic process (Park et al., 2006a; 2006b).

Lamb wave data are acquired using a commercial system that has a sampling frequency up to 25 MHz. The SHM algorithms for both hardware and signal processing are written in MatLab, which will be discussed in the next section. These algorithms control the entire process through the graphical user interface (GUI). An external amplifier (Krohn-Hite 7602M) is used to amplify the input signal to the PZT actuators.

In order to simulate damage in a reversible manner, industrial putty is affixed to the face of the panel in sizes ranging from 800 mm^2 to 1200 mm^2 (Fig. 2(e)). Reversible damage was first considered because the process allows to perform repeatable tests and to assess the performance of the data interrogation algorithms that will be described later. The damage identification methods are attempted for putty placed on the same side of the panel as are the piezoelectric transducers, as well as on the opposite side (Fig. 3). Irreversible damage is then inflicted on the panel by pressing a 6.35 mm square steel rod into the face of the panel. The load on the steel rod is increased to create larger areas of damage. The damage is applied slowly in order to prevent breaking or debonding of the PZT patches. To simulate more extreme damage scenarios, a screwdriver is used to create holes in the panel, first through only the face sheet opposite the sensors, then through the entire panel, shown in Figs. 8 and 9.

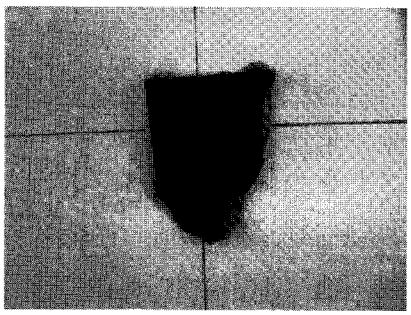

Fig. 3 A putty used in simulated damage for algorithm testing

3. Signal Processing Algorithms

Three signal processing algorithms are explored in this paper for use in SHM of honeycomb aluminum panels. The algorithms are written as MatLab functions and integrated by use of a MatLab GUI. The system is designed to communicate automatically with the data acquisition system, integrating the software and hardware components of the SHM system. Descriptions of the three algorithms follow.

3.1 Wavelet Attenuation

The first SHM technique presented in this paper takes advantage of the attenuation of Lamb waves. As Lamb waves propagate through a plate, the mechanical energy is dissipated through various processes that cause a decrease in the magnitude of the wave. The amount of attenuation between any two points in the plate will change when damage is introduced on the path between them. A comparison of the baseline signal and the test case yields the condition of the panel. This Lamb wave attenuation technique is based on that described by Sohn, et al. (2004) for detection of delaminations in composite structures.

The input waveform used is a five-peak Morlet wavelet, shown in Fig. 4. The experimentally derived driving frequency is 200 kHz in the 6.35 mm panel and 225 kHz in the 12.7 mm panel. These produce a well separated, S_0 mode, with a wave speed that is not overly adversely sensitive to small variations in frequency that might occur as the wave

propagates. In this case, the S_0 mode at the input frequency is used for damage detection because it has the highest group velocity at the input frequency and therefore, less susceptible to interference with reflected waves from the edge of the panel (Ihn and Chang, 2004). To achieve a better attenuation comparison between the baseline and test signals, both signals are transformed using the wavelet transformation. A more accurate wavelet transform is achieved by using a wavelet basis function that is the same as the input wave (Abbate et al., 1997; Lind et al., 2001). The wavelet transform, $Wf(u,s)$, is obtained by convolving the signal $f(t)$ with the translations (u) and dilations (s) of the mother wavelet

$$Wf(u,s) = \int_{-\infty}^{\infty} f(t)\frac{1}{\sqrt{s}}\psi^{*}_{u,s}(t)dt \ , \qquad (1)$$

where the base wavelet is given by,

$$\psi^{*}_{u,s}(t) = \frac{1}{\sqrt{s}}\psi(\frac{t-u}{s}) \ . \qquad (2)$$

The result of performing this operation yields the time-frequency response of the recorded signal. Only the component of the input driving frequency is of interest. The time response at the input frequency is recorded for both the baseline case and the test case. A comparison is made by use of a damage index(DI) based on a ratio of the kinetic energy of the test signal to that of the baseline signal, shown in eqn. (3),

$$DI = \frac{\left| \int_{u0}^{u1} Wf_t(u,s_0)du - \int_{u0}^{u1} Wf_b(u,s_0)du \right|}{\int_{u0}^{u1} Wf_b(u,s_0)du} \qquad (3)$$

In eqn. (3), subscripts b and t stand for the baseline and test signals respectively, and u_0 and $u1$ stand for the starting and ending time points for the first recorded S_0 mode. The DI ranges from zero, undamaged, and increases to a maximum value of one as the amount of attenuation increases. A more comprehensive description of this technique can be found in Sohn, et al. (2004). An appropriate damage threshold must be selected that will separate damaged path signals from undamaged signals. For this study, a threshold value of three standard deviations above the baseline-baseline damage index is experimentally derived.

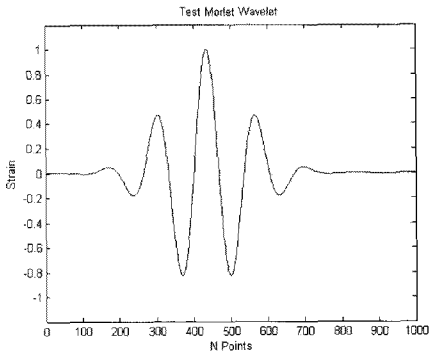

Fig. 4 Input Morlet wavelet

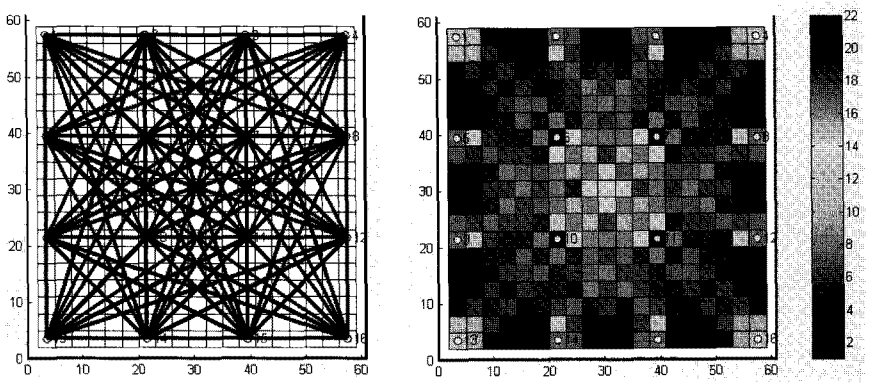

Fig. 5 Damage location grid with path crossings

When the damaged pathways between each of the piezoelectric transducer pairs are determined, they are plotted on a predefined grid. The total number of damaged paths intersecting each grid location is divided by the total number of undamaged paths intersecting that grid point. That result is normalized over the entire grid. The grid must be coarse enough to provide an adequate number of sensor path intersections for each element (Fig. 5). The normalized values are plotted on the grid in the user interface to indicate the most likely locations of damage to the panel.

3.2 Cross-Correlation of Power Spectral Density

A second technique employed for feature extraction from the recorded Lamb wave data involves the correlation of the power spectral density(PSD) functions between the baseline and the test case signals. The same Morlet wavelet that is used in the Lamb wave attenuation method is used to excite the panels. The dynamic response is recorded for every piezoelectric transducer pair path and the power spectral density for each of those signals is calculated. Although the panel is being actuated at only one driving frequency, the frequencies of the resulting Lamb waves are dependent on the thickness and material properties of the panel. Subtle variations in the panel thickness and the bond between the face sheets and core create different frequency components in the signal that is ultimately recorded, resulting in a frequency rich signal from which a meaningful PSD can be calculated. The damage index is based on the correlation coefficient of the PSD for the baseline signal versus the PSD of the test signal in a range around the driving frequency. Contrary to the wave attenuation, this method tracks the changes in the shape of propagated waves that can be caused by structural damage. Because a mere change in magnitude of the signal would not produce any damage indication, the correlation coefficient between baseline and tested signals is used as a damage sensitive feature. For consistency, the correlation coefficient is subtracted from one so that the signals with the highest correlation (i.e., indicate the least damage) have damage indices that approach zero, while signals with less correlation, indicating greater degrees of damage, will have greater damage indices with a maximum DI value of one, which is to remain constant with the damage index proposed in the wave attenuation method.

Once damage indices have been assigned to each path, a damage threshold is required to distinguish damaged path signals from the undamaged path signals. In the case of the cross-correlation of PSDs, a value of three standard deviations above the baseline-baseline damage index is considered damaged. The same grid and path based damage location algorithm is used for this method as is used for the wave attenuation model.

3.3 Triangulation of Reflected Waves

The third method for damage identification that is investigated utilizes the waves reflected from damaged sites in the panel. As Lamb waves propagate through a panel, they interact with defects in the structure, reflecting from the defect boundaries. These reflections are recorded by the piezoelectric transducers, acting as a sensor. A comparison between the test case and the baseline data reveals the presence and time

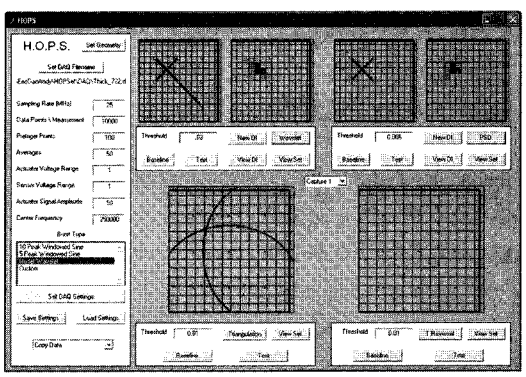

Fig. 6 Software graphical user interface

location of the reflected waves in the recorded signal. Time-of-flight can be used to for a wave of known velocity to determine the distance between the sensor and the defect. Using data from an array of sensors, the location of the defect can be triangulated.

The same baseline and test signals collected for the wavelet method are used for this method. However, only data recorded at the transducers in the corner positions of the array are used. The signals are first processed using the Wavelet transform, and the time response for the driving frequency is isolated in the same manner as for the wave attenuation algorithm. A Hilbert transform is then performed on the resulting signals creating a new curve that follows the peaks of the recorded signal in order to minimize the effects of minor misalignments in phase. The resulting signals are subtracted from each other leaving only the differences between the two signals. This result is normalized between zero and one with zero representing the case of no change between the baseline and test signals. A threshold value is determined below which changes are considered to be noise, not damage. Signals that occur before and during the normal first wave arrival are not considered as possible reflection candidates.

The damage can then be located using the time-of-flight data. The first point at which the normalized difference signal exceeds the threshold value is identified as the first arrival of waves deflected from the damage boundary. This signal is recorded as the time-of-flight for the reflected waves. The program calculates the wave velocity using the distance between actuating and sensing transducers, and the time between actuation of the signal and the arrival of the fundamental symmetric mode wave. The possible paths for the reflected wave define an ellipse around the sensing transducer according to eqn. (4).

$$x(\omega) = \frac{d^2 - p^2}{2(d\cos(\omega) - p)} \tag{4}$$

Where d is the distance between the actuator and the sensor, p is the path length traveled by the reflected wave, w is an angle that ranges from zero to 180 degrees, and x is the distance to the sensor. These ellipses are plotted for each of the corner transducers. The intersection of these ellipses defines the damaged area.

3.4 Software User Interface

A user graphical interface is created to merge the various Lamb wave signal processing method described, as shown in Fig. 6. Included also is the configuring the data acquisition system parameters, including sampling frequency, number of data points, number of averages, and input waveforms to be used for excitation in the structure. The interface displays the results from each of three damage identification algorithms for side by side comparison. This program is also designed in such a way that the measured data and the hardware parameters can be dynamically saved and loaded for the future analyses. By integrating hardware and several signal processing algorithms into one package, this approach creates an efficient SHM tool for various applications, allowing the uses to select the most suitable algorithm for different forms of damage in different applications. Although only honeycomb aluminum panel is investigated in this study, the software is designed and can be adapted into a variety of SHM techniques based on the use of active-sensing Lamb wave propagations.

4. Experimental Results

4.1 Wavelet Attenuation

The attenuation of the fundamental symmetric mode is found to be sensitive to both simulated damage as well as real damage. This method produces the greatest difference between the damaged case and the baseline case for

simulated damage in the form of industrial putty on the sensor side of the panel, as shown in Fig. 7. Sensor paths crossing the putty produce damage indices as large as 0.68. This method is less sensitive to putty on the opposite side of the panel from the sensors; in this case, the largest damage indices are on the order of 0.23. However, it is still possible to discern the damaged paths from the undamaged paths.

Real damage is then introduced into the

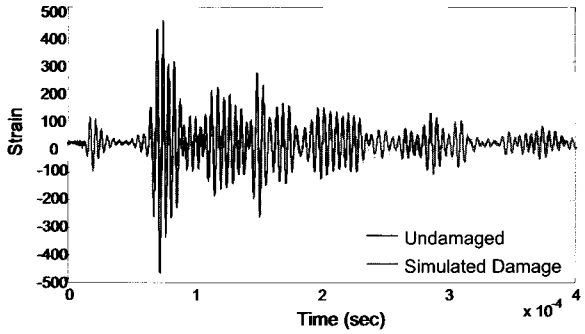

Fig. 7 Large attenuation caused by simulated dmage on sensor side of panel

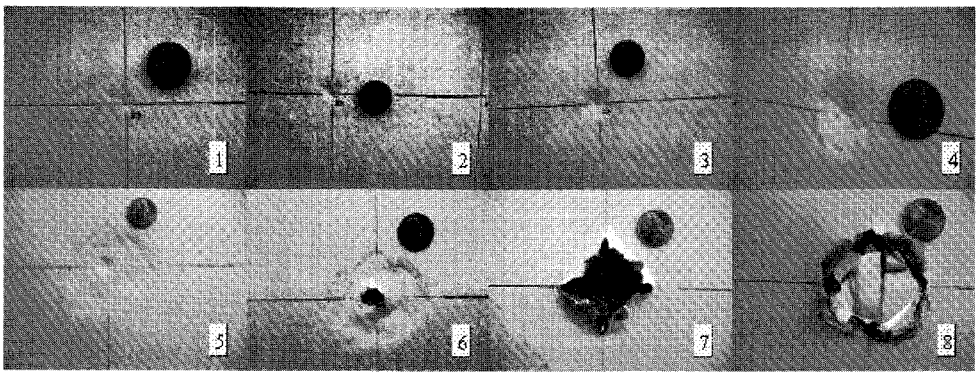

Fig. 8 6.25 mm panel damage cases 1-8. The damage cases 1-5 are small face wrinkles (one to eight cm in diameter) causing debonding of the honeycomb structure. Damage case 6 has a hole (0.5 cm diameter). Damage case 7 extends the holes in the front surface (2 cm in diameter) and Damage case 8 is the hole through the entire panel

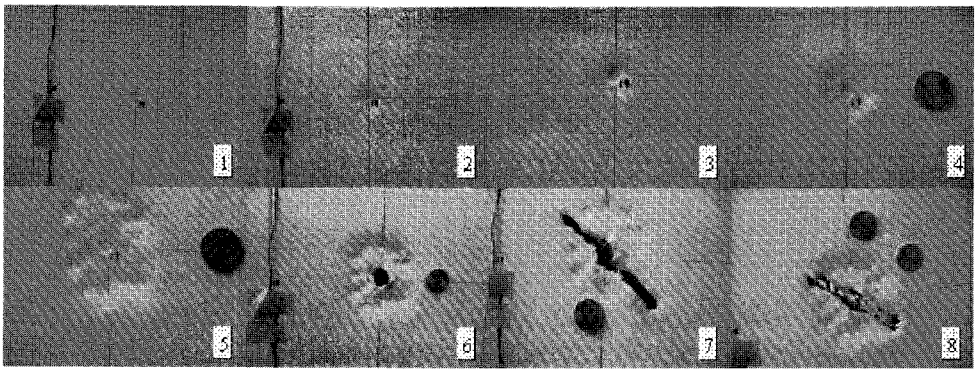

Fig. 9 12.7 mm panel damage cases 1-8. The damage cases 1-5 are small face wrinkles (one to eight cm in diameter) causing debonding of the honeycomb structure. Damage case 6 has a hole (0.5 cm diameter). Damage case 6 extends the holes into a notch on the front surface (8 cm in diameter) and Damage case 8 is the notch through the back face and finally through the entire panel

panel incrementally. For both panels, eight damage increments of increasing severity are used, as illustrated in Figs. 8 and 9. The damage ranges from small face wrinkles (one to three cm in diameter) to large face wrinkles causing debonding of the honeycomb structure (up to eight cm) to holes through the back face and finally through the entire panel. The resulting damage indices along each path for damage case 1 are summarized in Fig. 10 for the 12.7 mm panel; results for the 6.35 mm panel are similar.

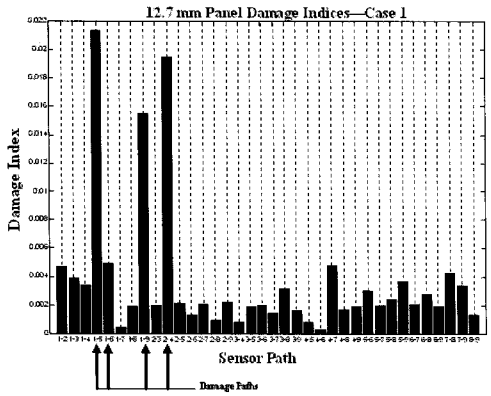

Fig. 10 Comparison of sensor path damage indices - damage case 1

For face wrinkling damage (cases one through five), the damage index is more sensitive to increases in the diameter of the wrinkle than increases in its depth. This is evident from the relatively large jump in the DI between damage cases one and two where the wrinkle is enlarged laterally and the lack of a jump in the DI between cases two and three where the depth of the wrinkle is increased. The DI actually drops when the first hole is created in the opposite side face sheet but increases again as the hole size increases. The largest damage indices are measured for case eight when the hole is propagated through the entire thickness of the plate.

The damage location algorithm successfully identifies the damaged paths in all damage cases for both plates. A summarization of the mean damage indices for damaged and undamaged paths for all cases is shown in Fig. 11. These paths are then used to locate the damage on a user-defined grid. The grid size used for this study is 30 mm by 30 mm. The state of damage for a given grid location is indicated by the intensity of the color displayed, which is a

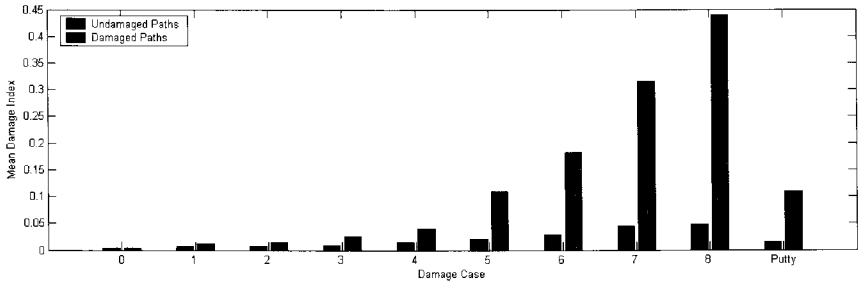

Fig. 11 Wavelet algorithm damage paths - mean damage indices for damage cases 1-8

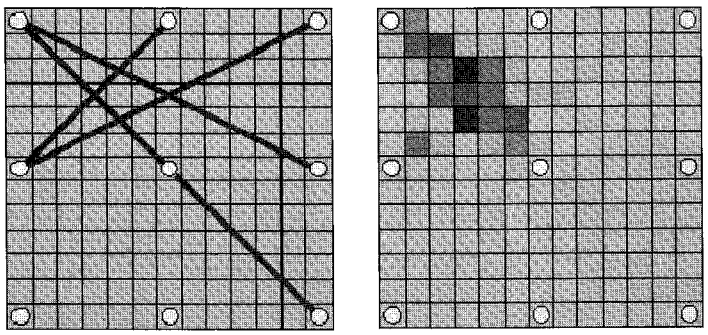

Fig. 12 Wavelet algorithm damage paths for damage case 7

function of the probability that that grid is damaged. The probability is based on the number of damaged paths intersecting the grid location versus the number of undamaged grid lines. The locations for the 12.7 mm panel of the calculated damage versus actual damage for each panel are shown in Fig. 12. Similar results are obtained for the 6.35 mm panel. Note that the damage index for the damage paths does not always increase as damage increases.

4.2 Cross-Correlation of Power Spectral Density

The PSD cross-correlation shows changes when simulated damage is applied to the panel as well as large face wrinkles and holes; however, it is less sensitive to small face wrinkles. In the 12.7 mm plate for damage cases one through four (small face wrinkles), the damage indices range between 0.03 and 0.09 for damaged paths and between 0.00 and 0.02 for the undamaged cases. The overlap makes it difficult to effectively separate the damaged paths from the undamaged paths. Cases one through four (large face wrinkles and holes), however, have damage indices ranging between 0.62 and 0.85 for damaged paths and between 0.08 and 0.18 for undamaged paths. These ranges allow for easy separation of damaged and undamaged paths by use of the damage index threshold value. Damage indices for the 12.7 mm panel for damage cases two and seven are presented in Fig. 13(a) and Fig. 13(b) respectively. The mean damage indices for the damaged paths using the cross-correlation of PSD are plotted for the 12.7 mm panel as a function of damage case in Fig. 14.

Damage indices for the 6.35 mm panel show the similar separation between the damaged and undamaged paths. The damage location is calculated using the same algorithm as is used for the wavelet-attenuation method. In cases

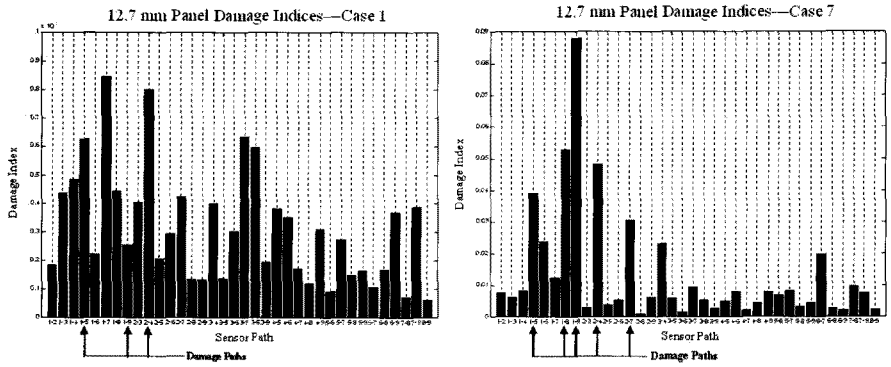

(a) (b)

Fig. 13 Power spectral density damage index for 12.7 mm panel; (a): noisy damage indices for damage case 1; (b) damage indices, damage case 7

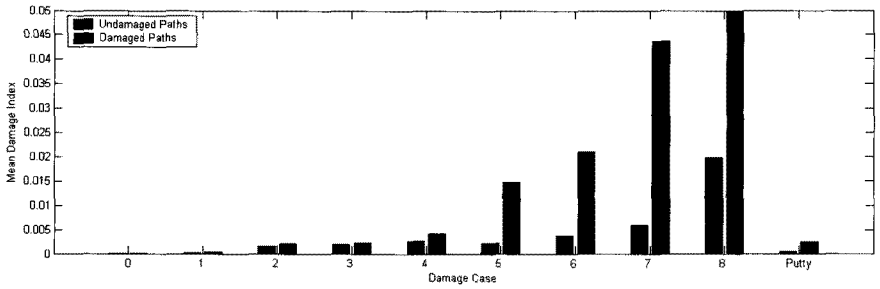

Fig. 14 Cross-correlation of PSD damage paths - mean damage indices for damage cases 1-8

where the damaged paths are distinguishable from the undamaged paths, the algorithm is able to locate the damage. Where there is little or no separation between damage indices, the algorithm fails. Though this method is less effective at locating damage as the wavelet attenuation method, the PSD damage indices along all paths increase reliably as damage increases, making this method more effective at characterizing the severity of damage.

One problem with the current implementation of this algorithm is that because the power spectral density is calculated over the entire length of the signal, reflections from the damage boundaries create differences in not only the damaged path signals, but the undamaged path signals as well. This means that as damage is introduced into the plate, the power spectral density of the damaged path signals change resulting in increases in the damage indices, but so do the signals for the undamaged paths. This drives up the damage indices for the undamaged paths as well, potentially leading to false positives along undamaged paths. Also investigated is the use of a sine sweep signal from 50 to 300 kHz because it has more frequency content than just a simple Morlet wavelet. The sine sweep does not produce noticeable improvements in the ability of the algorithm to identify damage.

4.3 Reflected Signal Triangulation

The algorithm for damage identification using signals reflected from damage boundaries is sensitive to holes in the face sheets, but less sensitive to face wrinkling and debonding. The damage indices for damage cases 1-5 are not significantly different than those for the baseline signal, shown in Fig. 15. It is not until holes are created in the panels, that the reflections become evident in the test case signal, as illustrated in Fig. 16. The location algorithm calculates a wave velocity of 498 m/s in the 12.7 mm panel for the fundamental symmetric Lamb wave mode and 462 m/s in the 6.35 mm panel, based on the arrival time and the distance between transducers. Using that velocity and eqn. (4), the location of the damage is triangulated and can be seen as the intersection of the ellipses surrounding the sensors in Fig. 17.

There are two primary problems encountered

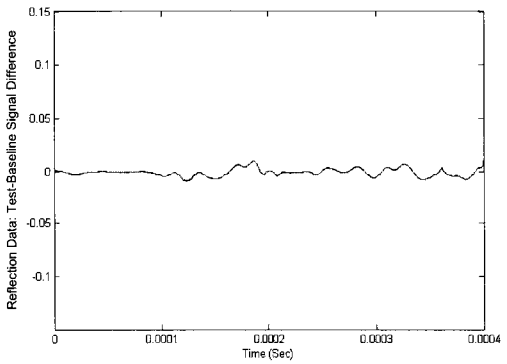

Fig. 15 Damage case 2: reflected waves indistinguishable from noise

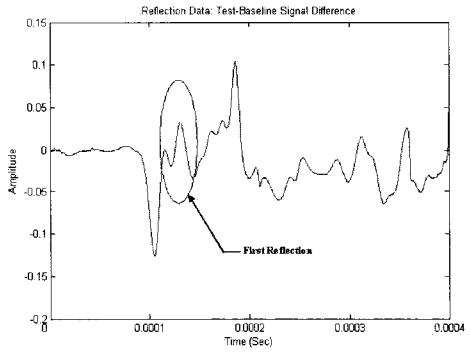

Fig. 16 Damage case 7: reflected waves visible

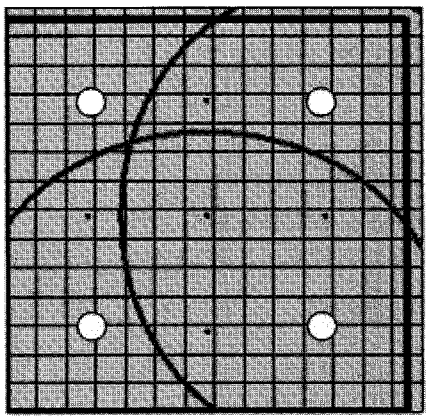

Fig. 17 Lamb wave triangulation

in interrogation of the signal reflections in the honeycomb aluminum panel application. First is the large number of reflections in the signal due to the honeycomb structure. This problem results in a relatively noisy difference signal, making small changes in the condition of the panel difficult to detect. Similarly, the plate boundary reflections also interfere with the damage boundary reflections. A more critical problem to the ability of the algorithm to identify damage is the anisotropic nature of the panel. It is observed that waves travel with different magnitudes and at different velocities depending on which direction they propagate through the panel. The result of these complications is a very complicate d signal in which many reflections not associated with damage are not satisfactorily cancelled out by the subtraction of the baseline signal from the test signal. The resulting signals are seen to exhibit damage indices that are more dependent on the direction a wave traveled than the presence or absence of any damage, making the full automation of the reflection algorithm for honeycomb aluminum panels nearly impossible as it is proposed.

5. Discussion

Specific topics that have not been extensively addressed in the SHM literature are i) the development of user friendly and automated software for data analysis; ii) coupling the sensing hardware directly with SHM data interrogation software. This paper is trying to address these issues, and the successful studies toward these areas will help to transition the current state-of-the-art of SHM to full-scale industrial adoption. By integrating three signal processing algorithms, an efficient SHM tool has been created that is generic and universal. Because each algorithm is sensitive to different forms of damage in different applications, the side by side comparison of their results provided by this approach is especially effective in allowing the analyst to identify damage. By integrating the software and hardware functions into one package and automating the process, the burden for the analyst is significantly reduced.

By employing a suite of SHM algorithms, this tool becomes a useful data interrogation program for a variety of plate structures. In the case of the honeycomb aluminum panels, the different algorithms produce varying degrees of efficacy. The wavelet attenuation analysis is particularly effective in identifying and locating damage. The cross-correlation of power spectral densities is not sensitive to small scale face wrinkling and debonding, however, because the entire received signal is interrogated, it has the potential to be a better tool to characterize the status of the entire system as well as the degree of damage. The reflected wave triangulation technique gives the fastest result using the fewest transducers, but is adversely sensitive to both reflections from the honeycomb structure and the effects of the anisotropic nature of the panel.

The relative sensitivities of these algorithms are likely to change for other plate structures in different applications. For instance, unlike anisotropic plates investigated in this study, the reflected wave triangulation method will be very effective in isotropic structures with a relatively fewer numbers of sensors installed, compared to other methods.

6. Conclusions

This study developed an automated and integrated Lamb wave-based active SHM system for honeycomb aluminum panels. The use of a suite of SHM signal processing algorithms provides the analyst with a richer output than would a single algorithm alone. The effectiveness of each of these signal processing algorithms for SHM in honeycomb aluminum panels under a variety of damage conditions is then compared and demonstrated. Although this study focuses on the monitoring of honeycomb aluminum panels only, the software developed in

this research can be adapted into a variety of structural health monitoring applications.

References

United States Department of Defense, Loading, Degradation and Repair of F-111 Bonded Honeycomb Sandwich Panels-Preliminary Study, Aug. 2000, DSTO-TR-1041, pp. 2-5

United States Government Accounting Office, Unmanned Aerial Vehicles: Progress of the Global Hawk Advanced Concept Technology Demonstration, April 2000, GAO/NSIAD-00-78, Washington: GAO, pp. 14

United States Government Accounting Office, Unmanned Aerial Vehicles: Major Management Issues Facing DOD's Development and Fielding Efforts, March 2004, GAO-04-530T, Washington: GAO, pp. 4

Abbate, A., Koay, J., Frankel, J., Schroefer, S. C. and Das, P. (1997), Signal Detection and Noise Suppression Using a Wavelet Transform Signal Processor: Applications to Ultrasonic Flaw Detection, 1997, *IEEE Transaction on Ultrasonics, Ferroelectrics, and Frequency Control*, Vol. 44, pp. 14-26

Bourasseau, N., Moulin, E., Delebarre, C. and Bonniau, P. (2000), Radome Health Monitoring with Lamb Waves: Experimental Approach, *NDT&E International*, Vol. 33, pp. 393-400

Diamanti, K., Soutis, C. and Hodgkinson, J. M. (2005), Nondestructive Inspection of Sandwich and Repaired Composite Laminated Structures, *Composites Science & Technology*, Vol. 65, pp. 2059-2067

Diamanti, K., Soutis, C. and Hodgkinson, J. M. (2005), Lamb Waves for the Nondestructive Inspection of Monolithic and Sandwich Composite Beams, *Composites A*, Vol. 36, pp. 189-195

Diamanti, K., Hodgkinson, J. M. and Soutis, C. (2004), Detection of Low-Velocity Impact Damage in Composite Plates Using Lamb Waves, *Structural Health Monitorin*, Vol. 3, pp. 33-41

Diaz Valdes, S. H. and Soutis, C. (2002), Real-Time Nondestructive Evaluation of Fibre Composite Laminates Using Low-Frequency Lamb Waves, *Journal of Acousti. Soiety of America*, Vol. 111, pp. 2026-2033

Farrar, C. R., Doebling, S. W. and Nix, D. A. (2001), Vibration-Based Structural Damage Identification, *Philosophical Transactions of the Royal Society: Mathematical, Physical & Engineering Science*, Vol. 359, pp. 131-149

Giurgiuti, V. (2005), Tuned Lamb-Wave Excitation and Detection with Piezoelectric Wafer Active Sensors or Structural Health Monitorin, *Journal of Intelligent Material Systems and Structures*, Vol. 16, pp. 291-306

Giurgiutiu, V., Zagrai, A. and Bao, J. J. (2002), Piezoelectric Wafer Embedded Active Sensors for Aging Aircraft Structural Health Monitoring, *International Journal of Structural Health Monitoring*, Vol. 1, pp. 41-61

Ihn, J. B. and Chang, F. K. (2004), Detection and Monitoring of Hidden Fatigue Crack Growth Using a Built-in Piezoelectric Sensor/Actuator Network: II. Validation Using Riveted Joints and Repair Patches, *Smart Materials and Structures*, Vol. 13, pp. 621-630

Kessler, S. S., Spearing, S. M. and Soutis, C. (2002), Damage Detection in Composite Materials Using Lamb Wave Methods, *Smart Materials and Structures*, Vol. 11, pp. 269-278

Lee, B. C. and Staszewski, W. J. (2003),

Modeling of Lamb Waves for Damage Detection in Metallic Structures: Part I. Wave Propagation, *Smart Materials and Structure*, Vol. 12, pp. 804-814

Lemistre, M. and Balageas, D. (2001), Structural Health Monitoring System Based on Diffracted Lamb Wave Analysis by Multi-resolution Processing, *Smart Materials and Structures*, Vol. 10, pp. 504-511

Lind, R., Kyle, S. and Brenner, M. (2001), Wavelet Analysis to Characterize Nonlinearities and Predict Limit Cycles of an Aeroelastic System, *Proceedings of AIAA/ASME/ASCE/AHS /ASC Structures, Structural Dynamics & Materials Conference*, pp. 337-356, Seattle, WA

Park, G., Farrar, C. R., Lnza di Scalea, F. and Coccia, S. S. (2006), Performance Assessment and Validation of Piezoelectric Active Sensors in Structural Health Monitoring, *Smart Materials and Structures*, Vol. 15, pp. 1673-1683

Park, G., Farrar, C. R., Rutherford, A. C. and Robertson, A. N. (2006), Piezoelectric Active Sensor Self-Diagnostics Using Electrical Admittance Measurements, *ASME Journal of Vibration and Acoustics*, Vol. 128, pp. 469-476

Qing, X. P., Chan, H. L., Beard, S. J., Ooi, T. K. and Marotta, S. A. (2006), Effect of Adhesive on the Performance of Piezoelectric Elements Used to Monitor Structural Health, *International Journal of Adhesion & Adhesives*, Vol. 26, pp. 622-628

Sohn, H., Park, G., Wait, J. R., Limback, N. P. and Farrar, C. R. (2004), Wavelet-Based Signal Processing for Detecting Delamination in Composite Plates, *Smart Materials and Structure*, Vol. 13, pp. 153-160

Worden, K. and Dulieu-Barton, J. M. (2004), An Overview of Intelligent Fault Detection in Systems and Structures," *International Journal of Structural Health Monitoring*, Vol. 3, pp. 85-98